PERFORMANCE ESTIMATION OF LINEAR TUBULAR ACTUATOR

*, **L. El Amraoui, *F. Gillon, *P. Brochet, **M. Benrejeb

* L2EP - Ecole Centrale de Lille, Cité Scientifique, B.P. 48, 59651 Villeneuve d'Ascq Cedex, France
** Unité de Recherche LARA Automatique, Ecole Nationale d'Ingénieurs de TunisBP. 37
le Belvédère 1002 Tunis, Tunisia

Key words

Dynamic simulation, finite element model linear tubular motor, reluctance network, test bench.

Abstract

The paper reports on the approach applied for linear tubular switched reluctance machine sizing, design and characterization. A prototype is built in order to validate the whole design process. Comparisons show a good agreement between computed and measured results. A response surface model of force versus position and current is then derived. This model allows an accurate prediction of the actuator performances.

1 Introduction

Linear motor drives are keyed to the need of a wide range in a variety of high and low power systems used in drive technology applications (cars, trains ..).
Using direct linear drives instead of rotating ones connected to rotary-to-linear devices and gearings is more practical and economic [1].
A growing interest in switched reluctance motors. This is because of the robust and simple structure of the motor and also because such motors appear to lend themselves to position control with relatively simpler drive systems as compared to induction motors[2]. In addition, the axi-symmetry of tubular structures, help to reduce the applied force on the actuator plunger to the propulsive tangential one.
Hence, linear tubular switched reluctance motors establish a simple and efficient solution for generating linear displacements [3].
The aim of this work is to achieve a linear tubular switched reluctance actuator with a fixed mechanical step and imposed starting force. This actuator can be used as an electric cylinder for linear drive. The mechanical step and the starting force values will depend on the application.
A reluctance network taking into account the saturation effects has been first developed in order to size the geometrical dimensions and electrical parameters of the machine [4].
The selected geometry is designed by finite elements and The energy method is used for static force characteristic computation [5]. Starting from the numerical design a prototype is built. Testing measurements validate the sizing and the global design approach.
A dynamic model of the machine is developed taking into account the force evolution versus position and current intensity and allowing that the machine's performance analysis.

2 Initial geometry

The structure selected for the actuator is a tubular one. Considering stator and plunger toothed structures with the same tooth and slot widths, four statoric phases are at least necessary for the machine to obtain a continuous displacement and a forward and backward-moving. Non magnetic separations must be set between the statoric phases so that only one statoric phase can be aligned with plunger teeth when it is supplied. Figure 1 shows the global structure of the linear tubular actuator.
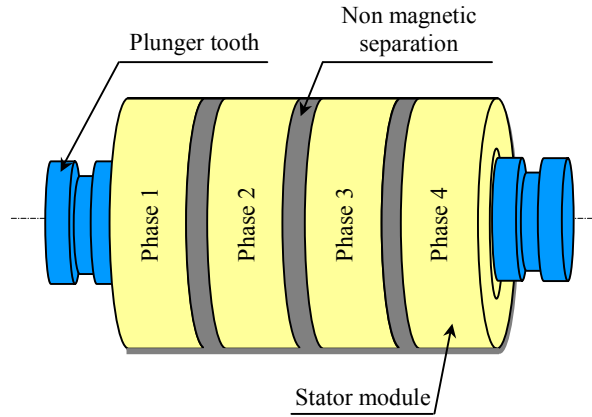
Fig. 1: Linear tubular structure of the actuator

The chosen structure is then a four-phase one, each exciting coil is winded around the plunger and lodged between two stator teeth.

With the assumption that the machine is perfectly axi-symmetric and that the statoric phases are not magnetically coupled, the construction of the actuator can then be obtained by assembly of elementary modules shown in axial plane on fig. 2.
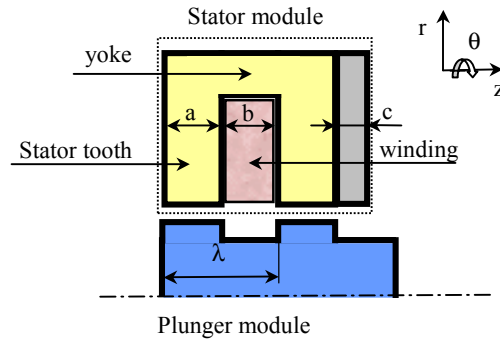
Fig. 2: Longitudinal half section of one actuator module

The plunger teeth are uniformly distributed and have a width equalling that of the stator tooth. So the supply of one phase translates the plunger of one step equalling half of a tooth width if the different phases are separated by an air gap equalling half the thickness of one tooth.

3 Reluctance network modeling

The geometrical sizing of the machine is done on two stages. The first stage is the axial sizing, it consists on the actuator axial dimension choice in accordance with the mechanical step. These dimensions are stator's and plunger's tooth (a) and slot (b) widths and also the non-magnetic separation thickness (c). The second stage consists on radial dimension computation with reference to the required propulsive force to be developed by the machine, the supply current, Joule losses and the magnetic saturation effects.

3.1 Axial sizing

The tooth-pitch of the machine λ is related to the mechanical step z_m, by equation (1) and also to the tooth and slot widths by equation (2), where N indicates the machine's phase number. Equation (3) explain the relation between the non-magnetic separation thickness and the slot and tooth widths.

$$z_m = \frac{\lambda}{N} = \frac{\lambda}{4} \tag{1}$$

$$\lambda = a + b \tag{2}$$

$$a = b = \frac{c}{2} \tag{3}$$

The selected structure is then defined by the mechanical step z_m chosen to 2.54 mm. Thus, according to equations (1) and (2), its tooth pitch λ is of 10.16 mm and because of equality between stator's and plunger's tooth widths, these two dimensions take for value 5.08mm while non-magnetic separation is of 2.54mm. In fact, the axial lengths are imposed by the chosen mechanical step.

3.2 Radial sizing

The actuator's radial sizing is more complicated than the axial one and strongly depends on the machine's magnetic state.
A non-linear reluctance network, taking into account the leakage flux into the slot, is built in order to calculate the magnetic quantities necessary for the machine design. Indeed, for a switched reluctance motor has got good performance it is necessary that it works in the magnetic saturation range [6]. An iterative process is used to correctly estimate the nonlinear reluctances [7]. Figure 3 shows the reluctance network achieved to obtain a first draft.
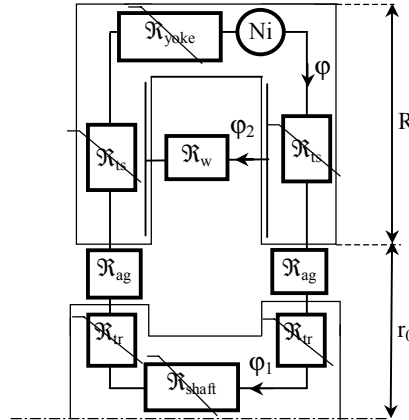
Fig. 3: Equivalent reluctance network

Magnetic saturation is taken into account by using the first magnetization curve in the non-linear iterative process. The discrepancy between the theoretical and practical results depends greatly on this characteristic[4].
The following analytical expression (4) is used to compute the material permeability μ_i versus the flux density B:

$$\frac{1}{\mu_i} = \frac{1}{\mu_0}\left(\varepsilon + (C - \varepsilon)\frac{B^{2\alpha}}{B^{2\alpha} + \tau}\right) \tag{4}$$

where C, τ, α and ε are least square coefficients determined from experimental B-H curve. Here, for the B-H curve of fig. 4, $\varepsilon = 1.1\ 10^{-4}$ C =1 α =5.23   and τ=7.02 10^4.
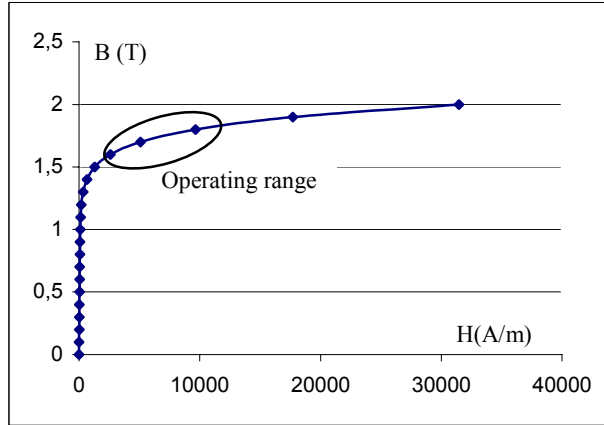
Fig. 4: B-H curve of the used magnetic material

The estimated value of μ_i is used to compute the reluctances $\mathfrak{R}_i$, in accordance with equation (5). The calculation is achieved by a successive substitution process allowing the permeability to vary with induction. Each reluctance $\mathfrak{R}_i$ of the main loop of the network (φ, $\varphi 1$), is computed by the classical expression:

$$\mathfrak{R}_i = \frac{1}{\mu_i} \frac{L_i}{A_i}$$ (5)

Where A_i the cross section area and L_i the full length, as shown on fig. 5. In the network, two kinds of reluctance are encountered: radial and axial ones, the reluctance length and area change following the kind of reluctance.

a. Radial reluctance   b. Axial reluctance
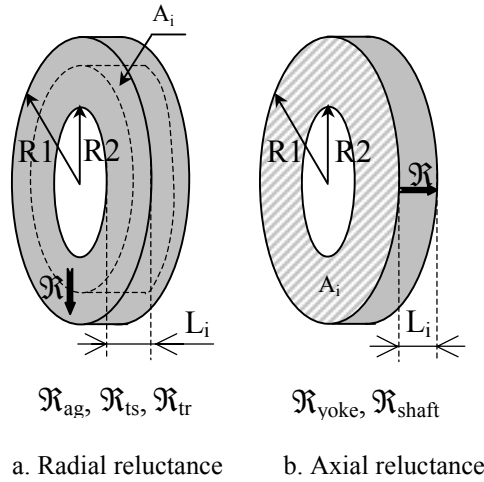
Fig. 5: Reluctance determination

Yoke and shaft reluctances are axial ones, air-gap and tooth reluctances are radial ones.
The leakage flux φ_2 through the slot is modelled by a specific reluctance because the flux is not uniformly distributed along the radius of the stator slot.
The leakage reluctance is given by :

$$\mathfrak{R}_w = \frac{6b}{\pi\mu_0 R(3R + 4r_0)}$$ (6)

where r_0 is the internal stator radius, R is the winding thickness. The thrust force developed by the actuator depends on the magnetomotive force (m.m.f.) distribution on the different parts of the machine. For switched

reluctance machines, the great part of the m.m.f. (ε) is concentrated on the air-gap. Hence, thrust force can be computed from the following expression [3,4]:

$$F_z = \frac{1}{2}\varepsilon_{ag}^2 \frac{1}{\mathfrak{R}_{ag}^2}\frac{d\mathfrak{R}_{ag}}{dz} \tag{7}$$

Where ε_{ag} is the air-gap m.m.f. and Fz the thrust force. This equation is obtained by an energy balance.

The actuator is required to develop a starting thrust force, corresponding to a shift of 50% between supplied stator phase and plunger teeth, of 20N. The actuator's structure is 10% oversized because the reluctance network model does not take into account the possible flux leakages through tooth sides. These leakages can decrease the useful force developed by the actuator.

The radial dimensions are determined from the parameterized reluctance network model. Some of them are imposed the other are deduced.

The average air-gap radius (R_{ag}) as well as the actuator's external radius (R_{ext}) are computed using a formulation having as objective the maximisation of the ratio of the ratio, static force by Joule losses, maximization [9].

Table 1. gives the radial sizes of the actuator, where, (y) is the stator yoke length and (Tr) the plunger tooth length.

Tab.1 radial dimensions

Geometrical parameters	Size (mm)
Average air-gap radius	15.05
Air-gap thickness	0.1
External radius	49
Stator yoke length	5
Plunger tooth length	4

Figure 11 gives the static thrust force evolution according to plunger shift, starting from an aligned position. This characteristic is obtained from non-linear iterative calculation by considering axial geometrical dimensions and a supply current of 300 Ampere turns in accordance with the thermal possibilities. The radial dimensions have been calculated so that the starting force is of 22N.
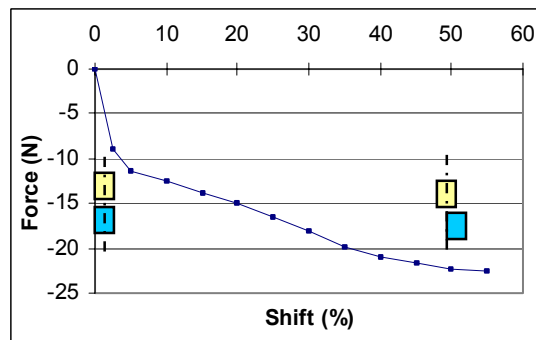
Fig. 6 : Thrust force given by reluctance network

4 Static characterization

4.1 Finite element Design

An axi-symmetric magnetostatic finite element model is built to analyze the machine's static behavior with more accuracy. In this model, the first magnetization curve of the plunger as well as the stator teeth and yoke are the same as that considered in the reluctance network model.

Fig. 7 shows the strong density of mesh necessary for the accuracy of the static force characteristic calculation.

In fact, to compute the thrust force with the Maxwell force tensor it is important to have a regular air-gap discretization and also a strong density of mesh. Some results have been computed with this method but an energy method is preferred for its robustness. Of course the two methods give similar results.
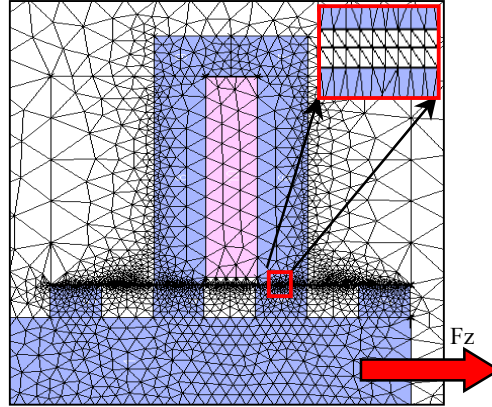
Fig. 7 : Finite element mesh

4.2 Electromagnetic force developed by the actuator

The co-energy concept is used to determine the electromagnetic force developed by the actuator; indeed, the electric equations governing the machine's operation can be described in the following matrix form:

$$[u] = [r][i] + \frac{d}{dt}[\phi] \tag{8}$$

where :
$[\phi]$: winding flux vector,
$[i]$: supply current vector,
$[u]$: terminal widing-voltage vecteur,
$[r]$: diagonal matrix of winding resistances.
Thus the total power developed by the electric sources providing the machine is given by [8]:

$$[i]^t [u] = [i]^t [r] [i] + [i]^t \frac{d}{dt}[\phi] \tag{9}$$

This power is distributed:
 - into magnetic energy variation stored in the machine $\frac{dW_m}{dt}$,
   - into Joule losses Pj dissipated in the windings:

$$P_j = [i]^t [r] [i] \tag{10}$$

- and into mechanical power P_{mec} provided to the outside, by means of the electromagnetic force Fz work as:

$$P_{mec} = Fz \frac{dz}{dt} \tag{11}$$

The equations (9), (10) and (11) are used to establish a power assessment and to evaluate the electromagnetic force work :

$$P_{mec} = Fz \frac{dz}{dt} = [i]^t \frac{d}{dt}[\phi] - \frac{dW_m}{dt} \tag{12}$$

Maybe under variational form:

$$Fz \, \partial z = [i]^t [\partial \phi] - \partial W_m \tag{13}$$

∂z can be regarded as an infinitesimal displacement carried out virtually in two possible ways:

- with constant flux $[\phi]$, so that, so equation (12) becomes :

$$Fz = \left(-\frac{\partial W_m}{\partial z} \right)_{[\phi]=cst} \tag{14}$$

- or with constant supply current $[i]$, so that equation (6) becomes :

$$Fz = \left(\frac{\partial \left([i]^t [\phi] - W_m \right)}{\partial z} \right)_{[i]=cst} = \left(\frac{\partial W_c}{\partial z} \right)_{[i]=cst} \tag{15}$$

The quantity $W_c = \left([i]^t [\phi] - W_m \right)$ of equation (15) represents the magnetic coenergy which is a virtual form of energy corresponding to the hatched part of figure 8. It is a concept easier than magnetic energy to be exploited for force computation. In fact, current control is easier than flux one. The machine's elementary step is of z_m, a small displacement ∂z of $z_m/8$ of the moving part is considered. A series of finite element simulations is launched on a static solver in order to compute the coenergy values for each position of the moving part over one electric period of λ. The average electromagnetic force values are then computed in accordance with equation (16) for elementary displacements Δz when one statoric phase is fed by a constant current.

$$Fz = \frac{\Delta W_c}{\Delta z} \tag{16}$$
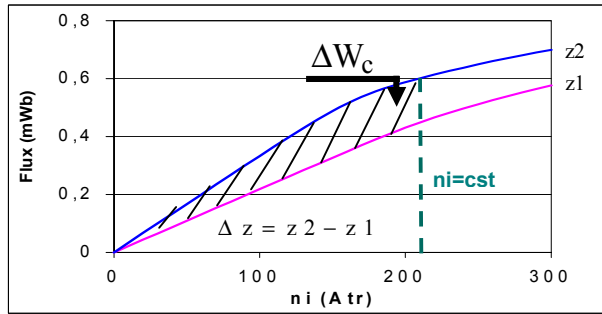
Fig. 8. Magnetic coenergy computation

The variations of the static force over one electric period are presented on fig. (9) for weak and strong saturation cases corresponding respectively to supply currents of 300 At, 600At and 900At.
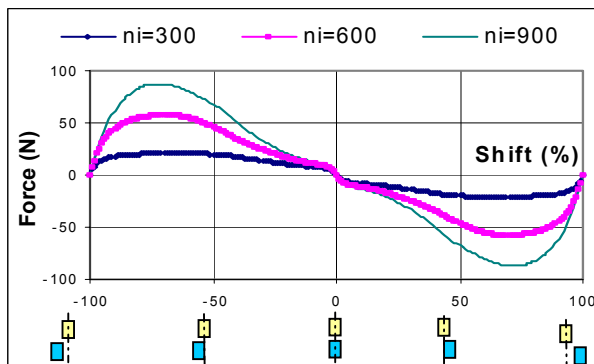
Fig. 9: Static force characteristics

As expected, for a supply current of 300At, the starting thrust force is of 20N. This result validates the dimensioning assumptions used for the reluctance network modelling.

The use of Maxwell stress tensor for force calculation leads to the same results as those obtained by the energy method except that the first method requires a strong density of mesh and regular air-gap discretization elements.

5 experimental data

5.1 Test bench

The test-bench presented on fig. 10 comprises the achieved prototype, force and displacement sensors. They are used, for the determination of the static force developed by the machine versus stator and plunger tooth shift starting from the aligned position and also for the determination of the dynamic response when one statoric phase is supplied.
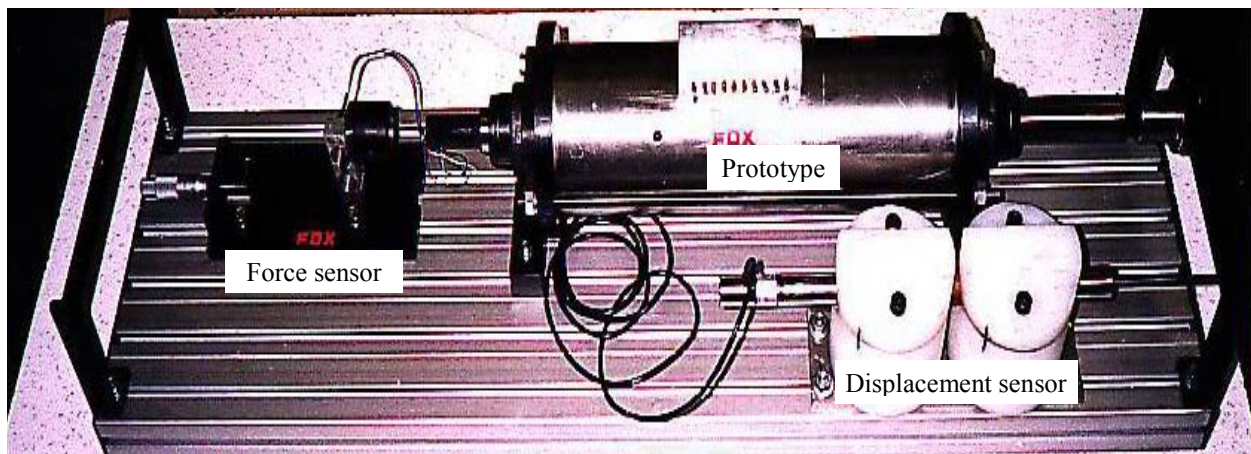
Fig. 10 : Test bench

A resistance strain gage is used for force measurement. The strain gage functions on the principle that when it undergoes strain, its electrical resistance changes. The electrical resistance strain gage is a strain-sensitive component bonded to the surface of a test part to measure strain. When the strain gage is stretched or strained, its resistance changes in direct proportion to the strain. By measuring the change in electrical resistance, the strain is also known.

A Linear Variable Differential Transformer (LVDT) is used for displacement measuring. It is an electromagnetic device that produces an electrical voltage proportional to the displacement of a movable magnetic core. It has a full range of 100 mm and a sensitivity of 102.64 mV/mm.

5.2 Static force characteristic

The force sensor as well as a micrometer caliper are placed in the actuator axis prolongation. The force sensor is fixed to a non deformable steel plate having the possibility to slip into the actuator moving part direction.

Thus, if an initial position corresponds to a steady balance of the actuator, and to a null effort contact between the plunger and the force sensor and also between the steel plate and the micrometer caliper, then a translation of the micrometer free extremity tends to move the plunger in the same way.

So, the actuator tends to maintain its balance position by applying an effort on the strain gauge.

For various positions of the moving part, measured with precision by use of the displacement sensor, the force exerted on the strain gauge is measured, providing then, the static characteristic of force of the machine versus position and supply current.

Figure 11 shows the static force characteristic determined in this way.
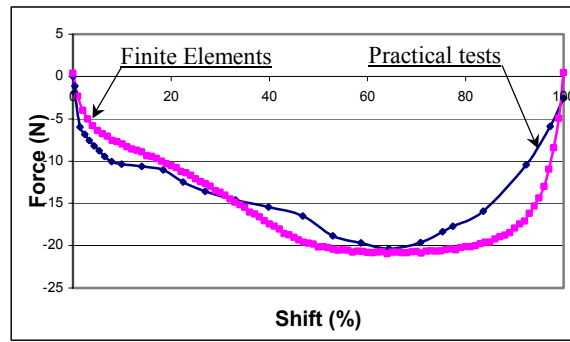
Fig. 11 : Static characteristic of force

The starting force is very closed to 20N. this result validates, on the one hand, the design method and, on the other hand, the finite element model used.

5.3 Dynamic response of the prototype

The mechanical step of the prototype is, actually, of 2.54mm. The measured step response is given on fig. 12.
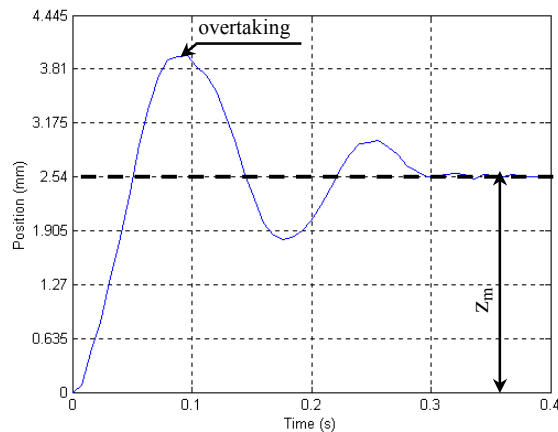
Fig. 12: Dynamic response of the prototype

The step motor oscillates around of its balance position before stabilization. In the test, an overtaking of about 60 % can be observed on the position response of fig.12. Following the load, the overtaking is more or less important.
The validation of simulations by experimental tests shows the efficiency of the different tools used for the machine sizing and design. Through the dynamic response

6 Dynamic behavior analysis

The linear tubular actuator is conceived for direct drive purpose, thus, the actuator performances depends,
not only, on its static characteristic but also on its dynamic behaviour which will be studied in this paragraph.

6.1 Mechanical equation

The dynamic response of fig. 12 corresponds to a non-linear model which can be described by the following scalar differential equation [6]:

$$ m \frac{d^2z}{dt^2} \ + \ \xi \frac{dz}{dt} \ + \ f_0 \, \text{sign}(\frac{dz}{dt}) \ = \ Fz - Fc \qquad (17) $$

where :

z : linear position   (m)

$\frac{dz}{dt}$: linear speed   (m/s)

$\dfrac{d^2z}{dt^2}$: linear acceleration (m/s^2)

m : load and plunger weight (Kg)

f$_0$: dray friction coefficient (N)

ξ : fluid friction coefficient (Ns/m)

Fz : electromagnetic force (N)

Fc : load force (N)

m, f$_0$ et ξ are constant intrinsic parameters of the actuator.

The synoptic diagram of the dynamic simulations carried on the no load linear motor is shown on fig. 13.
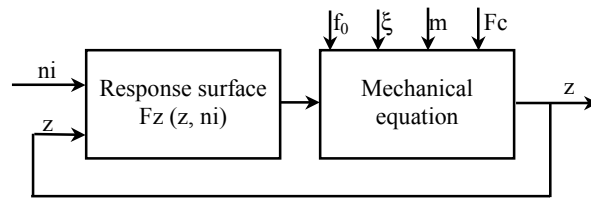
Fig. 13 : Synoptic diagram of the dynamic simulation

The efficiency of dynamic position simulation much depends on the numerical method used for the mechanical equation resolution as well as the static electromagnetic force characteristic estimation. Runge-Kutta at the 4th order is a powerful numerical method for such differential equation resolution [6]. To have the force according to the position and the current applied even for a saturated magnetic state, the actuator is modelled by the finite element method. These results are gathered within a response surface making up a continuous model of force, starting from a bi-dimensional interpolation. With this technique, the thrust force can be estimated for all positions and supply current values all over the operating domain.

6.2 Force response surface model versus position and supply current

For each, position of the plunger and supply current value, a model is build in order to estimate the electromagnetic force. Hence, the bi-directional space is subdivided into small interpolation elements. The actuator electromagnetic force is computed by finite element simulations done on 33 positions uniformly distributed over the electrical cycle (λ) and for three different values of supply current 300 At, 600 At and 900 At. The total simulation number is then equal to 99. Figure (14) shows the simulation point positions in the plane (phase current- plunger position).
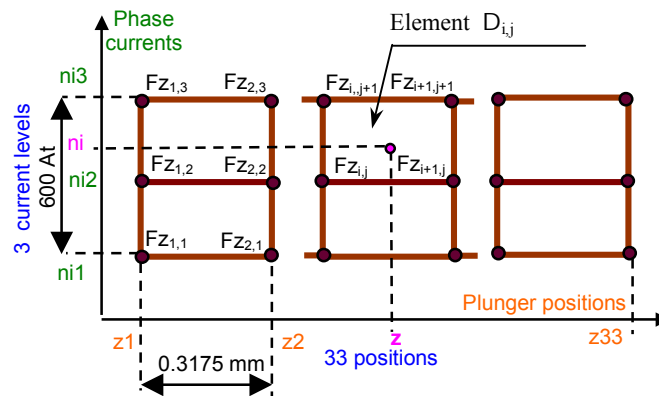
Fig. 14 : Simulation points position

Over each element D_{ij} of fig. 14, a linear interpolation model of the electromagnetic force is developed:

$$Fz\,(z,\,ni) = \mu + \alpha\,ni + \beta\,z + \delta\,z\,ni \qquad (18)$$

μ , α, β, δ are the model coefficients computed from the values taken by the electromagnetic force at the $D_{i,j}$ field tops: $Fz_{i,j}$, $Fz_{i,j+1}$, $Fz_{i+1,j}$ and $Fz_{i+1,j+1}$.

Thus, the thrust force response surface $Fz (z, ni)$, represented on fig. 15 is built for $ni \in [300, 900]$. For a null supply current, the thrust force is null for all plunger positions .
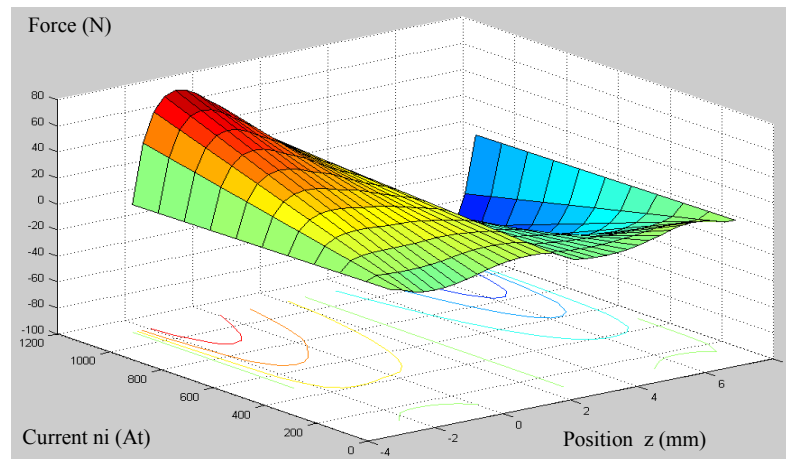
Fig. 15 : Thrust force response surface in versus current and position

This thrust force response surface allows then an electromagnetic force computation for any plunger position and phase supply current. The response surface model can be used, actually, to develop a step by step control strategy taking into account the magnetic saturation effect.

The accordance between the simulated dynamic response and practical one validates the machine's intrinsic parameter identification.

7 Conclusion

The achieved linear tubular switched reluctance machine have a regular mechanical step of 2.54 mm and can develop a starting force of almost 20N. These results validate the modeling approaches. The reliable tools developed here will then allow to identify the actuator intrinsic parameters and also to optimize its geometrical dimensions.

8 Acknowledgement

9 References

1. C.B. Rajanathan and G.Hu " A novel tubular linear induction actuator ", ICEM 92 Vol 1, pp. 137-140.

2. H. Bülent Ertan " Precision of torque and inductance displacement characteristics of asymmetrically slotted variable-reluctance motors using a simplified model for numerical field solution " IEEE Transactions on magnetics, vol.35, NO. 5, September 1999.

3. L. El Amraoui, F. Gillon, P. Brochet et M. Benrejeb, "Design of linear tubular step motor", Electromotion'01, Vol. 1, pp.223-227.

4. M. Jufer, "Traité d'électricité, électromécanique", Presses Polytechniques et Universitaires Romandes, Lausanne 1995.

5. I. Nathan, P.A. Joao " Electromagnetics and calculation of fields", Springer-Verlag, New York, 1992.

6. T.J.E. Miller, "Brushless Permanent Magnet and Reluctance Motor Drives", Oxford Science Publications, 1989.

7. H. Roisse, M. Hecquet, P. Brochet, 'Simulations of synchronous machines using electric-magnetic coupled network model' , IEEE Trans. On Magnetics, Vol. 34, No 5, pp 3214-3217, September 1998

8. Mailfert A. "Machines à reluctance variable", Techniques de l'Ingénieur, traité génie électrique, D550, 1986.

9. E. Hoang, Y. Amara, M. Lecrivain, M. Gabsi "machine synchrone à aimants Permanents Structure à Commutation et à Concentration de flux Principes et résultats Expérimentaux", EF'2002 Nancy.